치의학석사 학위논문

아녹타민 아형의 클로닝과 이종발현 연구

Cloning and Heterologous Expression of Anoctamin Isoforms

2013 년 2 월

서울대학교 대학원
치의학대학원 치의학과
박 한 검

아녹타민 아형의 클로닝과 이종발현 연구

Cloning and Heterologous Expression of Anoctamin Isoforms

지도교수 **Frank Hong Yu**

이 논문을 치의학 석사학위논문으로 제출함

2012년 11월

서울대학교 대학원

치의학대학원 치의학과

박 한 검

박한검의 석사학위논문을 인준함

2012년 12월

위 원 장 노 상 호 (인)

부위원장 서 덕 규 (인)

위 원 **Frank Hong Yu** (인)

Abstract

Cloning and Heterologous Expression of Anoctamin Isoforms

Hankum Park
Department of Dentistry
The Graduate School
Seoul National University

Anoctamin1 (Ano1) has Ca^{2+}-activated Cl^- channel (CaCC) character which has an important role in salivation. There are nine other members in the anoctamin family, and not much is known about them except Ano1. In this study, mouse Anoctamin9 (mAno9) and human Anoctamin6 (hAno6) gene were cloned, epitope tagged with enhanced green fluorescent protein (EGFP) or hemagglutinin (HA) tag to the C-terminus, and heterologously expressed in human embryonic kidney (HEK) 293 cell. Consequently, location of the expressed EGFP-linked anoctamin channel proteins in the cell was examined and proteins were extracted in order to detect anoctamin protein with EGFP-specific antibody. As a result, both mAno9 and hAno6 cDNA expression plasmids were heterologously expressed in HEK293 cell. mAno9 appeared to be intracellularly localized in an uniformly diffuse pattern, while hAno6 was expressed in both plasma membrane and intracellular compartments, suggesting distinct roles within the cellular compartments.

Keywords: anoctamin, Ca^{2+}-activated Cl^- channel, cloning, heterologous expression
Student number : 2009-22686

Contents

Tables

Figures

Introduction

Human body secretes approximately one liter of saliva a day. Although water forms 94 to 99.5 weight percent of this fluid, saliva also contains important inorganic ions, such as Na^{+}, K^{+}, Ca^{2+}, Cl^{-} HCO_3^{-}, $H_2PO_4^{-}$, and HPO_4^{2-}, and organic components such as urea, amino acids, glucose, lactate, fatty acids, and proteins including amylase, albumin, immunoglobulin, lysozyme, and lactoferrin [1]. Their composition and concentration of constituents vary depending on the secretion rate, relative contribution among salivary glands, or mode of salivary gland stimulation of secretion.

Saliva has essential roles in oral health. It initiates digestion of food as amylase hydrolyzes α-1,4-glycosidic bonds of carbohydrates. Additionally, lubricative property of saliva protects oral tissues and helps swallowing of the masticated food. Moreover, continuous secretion of saliva clears food debris and microbes from the teeth and oral cavity, providing less conducive microenvironment for the development of dental caries, periodontitis, and halitosis. Calcium and phosphate ions present in saliva are required for enamel to be remineralized, which is an important compensatory process to save tooth structure from being dissolved in locally bacteria-induced acidic condition. In patients with dentures, saliva provides the surface tension force that contributes to the retention of the dentures [2].

Importance of saliva in oral health is underscored by the many clinical problems that arise from loss or decrease in salivary seceretion. Xerostomia is one such prevalent oral concern in many patients where the subjective feeling of dry mouth is caused by a severe reduction of salivary flow. It is associated with numerous systemic diseases and conditions such as prescribed medications, autoimmune diseases, and radiation treatments to head and neck. It is presumed that up to 10 percent of the general population experiences persistent dry mouth feeling [3]. It is more frequently complained with increasing age, and over 25

percent of older patients suffer from dryness oral cavity [3]. Xerostomia is most frequently associated with altered salivary gland function and can lead to many oral complications because of the essential roles of saliva in oral health.

Salivary secretion

There are major salivary glands and minor salivary glands. The major ones are composed of parotid gland, submandibular gland, and sublingual gland. The minor ones include palatinal, buccal, labial, lingual, and retromolar gland. Parotid gland has acinar cell of serous type. It is innervated by glossopharyngeal nerve and supplied by transverse facial artery. Submandibular and sublingual gland have both serous and mucous cell and are innervated by facial nerve. The former is supplied by facial artery, while the latter is supplied by sublingual artery. Palatinal, buccal, labial, and some part of retromolar gland are mucous type and innervated by facial nerve, whereas lingual, and the other part of retromolar gland are serous type and innvervated by glossopharyngeal nerve [1].

Salivary glands are controlled by both sympathetic and parasympathetic nerves. Postsynaptic terminal of sympathetic nerve terminals release norepinephrine which binds to alpha- and beta-adrenergic receptor located at basolateral side of acinar cell. Excitation of sympathetic nerve facilitates vigorous secretion of proteins and mucin because there are plenty of β-adrenergic receptors at basolateral portion of submandibular and sublingual gland acinar cells. However, serous salivary secretion from parotid gland gets weak with sympathetic stimulation because parotid acinar cell has parasympathetic receptor dominantly. On the other hand, acetylcholine from parasympathetic nerve terminal binds to muscarinic receptor and stimulates secretion of serous saliva from parotid gland.

Acetylcholine signal from the parasympathetic nerves activates muscarinic G-protein coupled receptor, which in turn stimulates phospholipase C and hydrolyzes phosphatidylinositol 4,5-bisphosphate (PIP_2) into diacylglycerol (DAG) and

inositol 1,4,5-trisphosphate(IP_3). IP_3 activates the endoplasmic reticulum (ER)-located Ca^{2+} release channels that increases $[Ca^{2+}]_i$ via release from the ER store. The intracellular Ca^{2+} increase results in the following three effects. Firstly, it opens Ca^{2+}-activated K^+ channel at basolateral membrane of acinar cell. Secondly, it activates Cl^- channel at luminal membrane and increases permeability of Cl^-. Thirdly, it leads the secretory granules to move toward luminal membrane and causes exocytosis. The increase of $[K^+]_i$ from the first result activates $Na^+/K^+/2Cl^-$ cotransporter (NKCC1) and elevates the concentrations of sodium, potassium, and chloride ions. Energy source of NKCC1 is the $[Na^+]$ gradient maintained by Na^+-K^+ pump. The basolaterally entered Cl^- exits to the lumen through Cl^- channel and Na^+ moves into the lumen via tight junction to maintain charge balance. As the Na^+ and Cl^- ions are osmotically active, the resulting osmolarity gradient drives movement of water through aquaporin of the luminal membrane to result in the secretion of the isotonic initial acinar fluid. Figure 1 illustrates a model depicting the mechanism of acinar cell secreting fluid and electrolytes [4].

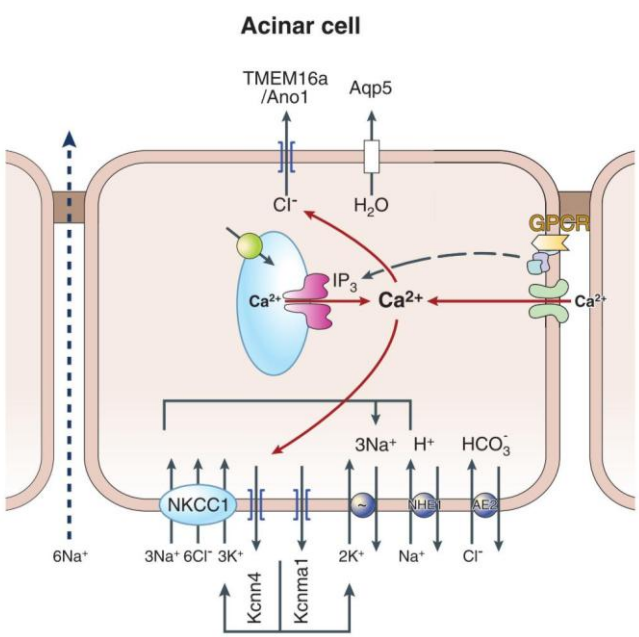

Figure 1 A model describing the mechanism of acinar cell fluid and electrolyte secretion (Figure from reference [4]).

Then ductal cells modify composition of the fluid [1]. At the luminal side membrane of dutal cells, there are Na^+ channel, Cl^- channel, HCO_3^- exchanger, Na^+/H^+ exchanger, and K^+/H^+ exchanger. They selectively absorb Na^+ and Cl^- ions into ductal cells while K^+ and $HCO3^-$ ions are secreted into lumen. Because water remains in the lumen, the salivary fluid becomes hypotonic. Meanwhile, there are Na^+-K^+ pump, Na^+/H^+ exchanger, K^+ channel, and Cl^- channel at the interstitial side membrane and they pump Na^+ out to maintain Na^+ gradient across luminal fluid and ductal cells. As a result, Na^+ can move from luminal fluid to ductal cell and Cl^- follows Na^+ to balance electric charge. Increase of Ca^+ that is required for ductal cell activity occurs as acetylcholine acceptor and α-adrenalin receptor are stimulated.

Calcium-activated Chloride Channel – Anoctamin 1

It had long been considered that Cl^- exits acinar cells by a conductive pathway which was later demonstrated as an apical Ca^{2+}-activated Cl^- channel (CaCC) [5]. There are at least two functions that can be fulfilled by CaCCs where they are expressed. First, CaCCs may perform a role in Cl^- movements for some epithelial cells whose activation would lead to transepithelial transport of salt together with water. Second, they shift membrane potential, which has an effect on excitability in neurons including the modulation of transduction in sensory neurons [6].

The major electrophysiological characteristics of classical CaCCs were studied in lacrimal glands. In this tissue, the CaCCs are activated by intracellular Ca^{2+} in the range of 0.5 to 2μM with a steep dose-response curve suggestive of cooperativity [7]. Through this channel, chloride currents flow more easily in the outward direction (during depolarization) than inward, and is so-called outwardly rectifying channel. Under CaCC currents are activated by depolarization at low intracellular Ca^{2+}. However, the channels became virtually voltage-insensitive and non-rectifying at the higher 2μM intracellular Ca^{2+}. Later, it was reported that similar currents found in salivary parotid acinar cells and proposed them as the

mediators of Cl^- efflux activated by increased intracellular Ca^{2+} during fluid secretion [5].

Recently, three independent research groups have identified TMEM16A as the CaCC in several cell types by different methods [8-10]. Yang et al datamined public domain databases for genes coding for putative transporter or channel proteins of unknown function with more than two predicted transmembrane domains [8]. Caputo et al searched for possible enhanced transcribed genes in microarray analyses based on their earlier observation that long-term stimulation with cytokines from human bronchial cells results in the enhancement of calcium-dependent chloride secretion activated by UTP [8]. Schroeder et al utilized the fact that oocytes from the axolotl, *Ambystoma mexicanum*, lack CaCCs and used this experimental model as an expression cloning system to clone *Xenopus laevis* oocyte CaCC mRNA [9]. They found xTMEM16A, the expression of which generated calcium-activated chloride currents with typical marked voltage dependence and outward rectification of Xenopus oocyte CaCC. Schroeder et al also identified the mouse isoform of TMEM16A, showing its functional expression in HEK293 cells, and demonstrated the presence of TMEM16A mRNA in mammary and salivary glands by *in situ* hybridization.

The importance of TMEM16A in salivary secretion was demonstrated as it was expressed highly in the luminal part of salivary acinar cells [9], as the knockdown of TMEM16A by siRNA depleted salivary secretion [10], and as the knockout of TMEM16A eliminated the CaCC activity in acinar cells [11].

Figure 2 compares Ca^{2+}-activated Cl^- currents in HEK cells transfected with Ano1 to native inner medullary collecting duct (IMCD) cells [12]. In both cells, currents are activated slowly with time, are outwardly rectifying, and show de-activating tail currents upon repolarization. The time course of activation of the current in IMCD cells however is generally slower than the Ano1-transfected cells. This fact suggests that another Ano subfamily or other subunits may be involved in the native currents found in IMCD cells. Nevertheless, the anion current induced

by Ano1 is much more similar in appearance to native CaCCs than any other candidate.

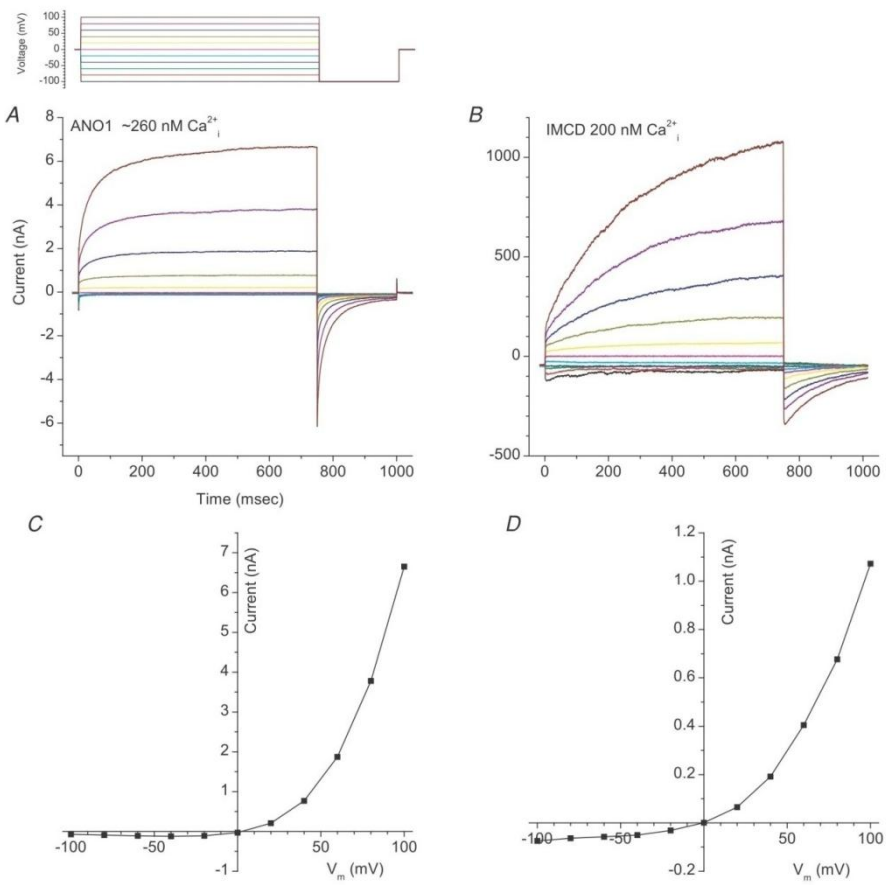

Figure 2 Ca^{2+}-activated Cl^- currents. The voltage clamp protocol is shown above A. A and B, currents from HEK-cells transfected with Ano1 (A) and native IMCD cells, respectively. (B). C and D, I-V curves measured at the end of the test pulse in A and B, respectively (Figure from reference [12]).

After discovering of the anion channel nature of TMEM16A, Yang et al proposed to change the name of TMEM16A to Anoctamin (Ano) for, ANion channels with eight (OCT) transmembrane segment proteIN. Figure 3 shows Ano1 structural topology of 8 transmembrane domains (TMDs) and a pore loop

containing several cysteine and charged amino acid residues [13]. Ano1 contains a non-canonical calmodulin (CAM) binding sites at N-terminus [13], and has a domain of five consecutive glutamic acid residues that is reminiscent of the Ca^{2+} bowl of the large conductance Ca^{2+}-activated K^{+} channel that is involved in Ca^{2+} binding [14].

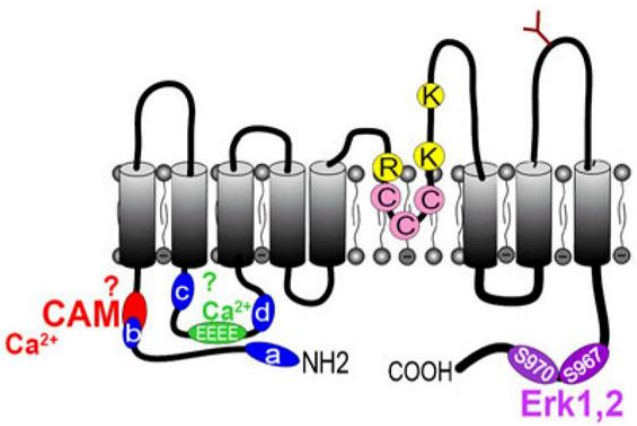

Figure 3 Model of Ano1 having eight transmembrane helix domains and a pore loop with several cysteine and charged amino acid residues. Ano1 is alternatively spliced as indicated with blue ovals, and may contain non-canonical CAM binding sites in the N-terminus (Figure from reference [13]).

Anoctamin family

Members of the anoctamin family are found throughout the eukaryotes, including mammals, flies, worms, plants, protozoa and yeast and phylogeny of anoctamin family is shown in Figure 4. However, they seem best represented in the higher vertebrates. Mammals have 10 gene members. The sequence homology within the putative pore region of anoctamins is considerable, while the overall homology is only moderate [15]. Ano1 and Ano2 (TMEM16B) are closely related about 60% of amino acid identity. However, the other anoctamins have identity of 30% or below [13].

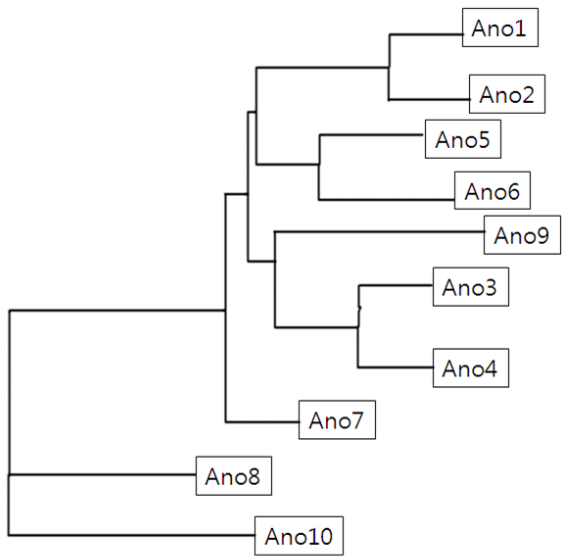

Figure 4 Phylogeny of Ano family [12]. The tree was constructed using the fast minimal evolution method [16].

A detailed analysis of expression of ten anoctamins indicated that every cell type in mouse and human tissues expresses at least two, but often several different anoctamin isoforms [17]. Expression of Ano RNAs in mouse tissues is illustrated in Figure 5. Ano6 and 10 are broadly expressed in mouse and human tissues, and Ano6 is the most abundant paralog. Ano8 is widely expressed although at lower levels. Ano2, 3, and 4 are preferentially expressed in sensory receptor cells and neuronal tissues, while Ano5 was found in skeletal muscle and thyroid gland.

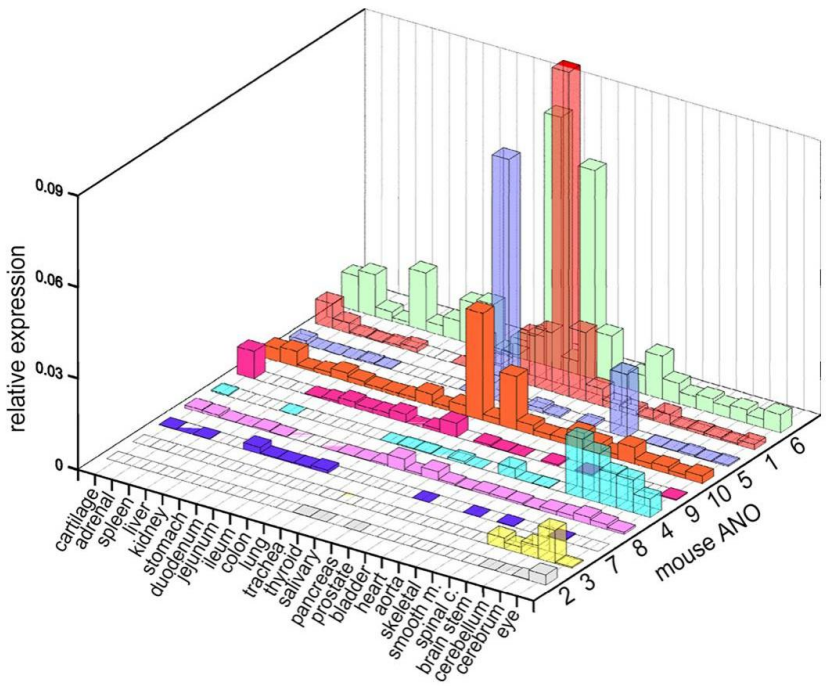

Figure 5 Expression of Ano RNAs in murine tissues. Real-time RT-PCR was performed from total RNA of different mouse tissues [17].

So far, Ano1 and Ano2 have been clearly shown to have Cl^- channel activity [10, 18]. It was also reported that Ca^{2+}-activated Cl^- current was generated by Ano6 and Ano7, while Ano5, 8, and 10 did not produce any measurable currents [17]. Interestingly, it is known that the activity of Ano1 is reduced by coexpression of Ano9 with Ano1 into Fisher rat thyroid (FRT) cells by transient transfection, suggesting that these two isoforms may functionally interact in the plasma membrane.

It is also entirely possible that anoctamins have diverse functions either as plasma membrane localized proteins or intracellular compartments. For example, Ano6 was found to induce scramblase activity in platelets [19]. Phospholipids are asymmetrically distributed between the outer and inner leaflets of plasma membrane [20], and scramblase mediates the bidirectional transfer between plasma

membrane leaflets of all phospholipids. This asymmetric distribution is disrupted in many biological systems. As an example, activated platelets expose phosphatidylserine to trigger the clotting systems. A defect in phospholipid scrambling activity is found in a congenital bleeding disorder, Scott syndrome [21] [22]. The syndrome is caused by a mutation at a splice-acceptor site of the gene coding Ano6, causing the premature termination of protein, leading to nonfunctional Ano6 [19].

Anoctamin-related diseases

It is known that Ano1-knockout animals lead to multiple defects in epithelial organs such as an airway, salivary glands, pancreatic glands, hepatobiliary tract, and large intestine. Some examples of expression, function, and role in disease are listed in Table 1. CaCC regulates myogenic tone and contraction stimulated by agonist in vascular smooth muscle, supports contraction in visceral smooth muscle, fertilizes potential after sperm fusion to prevent polyspermy in oocytes, and causes cell shrinkage in blood coagulation [13].

Table 1 Expression, function, and role in disease of anoctamins (Table from reference [13]).

Tissue	Function of CaCC	Ano	Role in disease
Vascular SM	Regulates both myogenic tone and contraction stimulated by agonists	1,6,10	Role in hypertension is likely
Endothelium	Regulation of $[Ca^{2+}]_i$ and NO-synthesis	1	Platelet adhesion defects
Visceral SM Cajal cells	Support contraction. Ano1 highly expressed in non-neuronal non-muscular Cajal cells, SMC of epididymis, and oviduct	1	GIST, squamous carcinoma, head and neck cancer, Defective SM contraction, Diabetic gastroparesis. Asthma
Heart	Repolarization from action potential	4,5	
Neuronal tissue	Hyperpolarization or depolarization, Pain perception by nociceptive sensory neurons	2,3,4,6,8,10	Autosomal-recessive cerebellar ataxia, Panic disorder
Skeletal M; skeleton	Role unknown	1, 5, 6, 10	Limb-girdle M dystrophy, myopathy gnathodiaphyseal dysplasia
Airways, Alveoli	Cl^- secretion. Secretion and absorption in alveolar type II cells	1,6 9,8,10	Cartilage malformation, reduced mucociliary clearance.
Colon	Age-dependent Cl^- secretion, volume regulation.	1,6,7,9,10	Anoctamins may play a role during rotavirus diarrhea and in colonic cancer.
Glands	Transport in acini and ducts of pancreas, salivary gland, airway submucosal and lacrimal glands	1,6,8,9,10	Impaired saliva production prostate cancer
Kidney	Role CaCC in the kidney obscure. Most studies performed in cultured cells and not in native tissues	1,6,10	
Biliary epithelium, Liver	CaCC important for bile formation	1,6,10	
Olfactory receptors	Receptors maintain a high internal Cl^-, Opening causes depolarization	2	
Taste receptor	CaCC activity hyperpolarizes the receptors, taste adaptation	7	
Inner ear	Role unknown	2	Nonsyndromic hearing impairment
Retina	Synaptic transmission of the photoreceptor signal in ret. pig. epith.	2	
Oocytes	Fertilization potential after sperm fusion to prevent polyspermy	1	
Blood, Coagulation	ANO 1 important for cell shrinkage	1	Role in hemolysis, Willebrand disease type 3

Another interesting feature of anoctamin family is that they are upregulated in various cancers [23]. Before Ano1 was discovered as CaCC, it had been known as cancer-associated protein in gastrointestinal stromal tumors (GISTs) and head and neck squamous cell carcinomas [23-25]. In this reason, Ano1 was called DOG1 (discovered on gastrointestinal stromal tumor 1), TAOS2 (tumor amplified and overexpressed sequence 2), and ORAOV2 (oral cancer overexpressed 2). Although Ano1 may not be the cause of the tumor, its function may support tumor progression. Ano1 is located on chromosome 11q13 and appears that amplification of this chromosomal region occurs in many tumors including almost half of oral squamous cell carcinomas, where it has been correlated with a poor outcome [26], and human neck squamous cell carcinomas [23]. Ano7, also known as NGEP is expressed on the apical and lateral membranes of normal prostate and prostate cancer cells and at cell-cell junctions of the LNCaP prostate cancer cell line [27]. Moreover, splicing variants of Ano6 are associated with metastatic capability of mammary cancers in mouse and is associated with poor prognosis of patients with breast cancer [28].

Identification of anoctamin family as calcium-activated chloride channel candidate involved in exocrine secretion has spurred an active investigation to discover the function and physiological relevance of the anoctamin family. Two members of this anoctamin protein family were the focus of the present thesis: mouse Ano9 (mAno9) and human Ano6 (hAno6). These members are of interest because Ano6 is a most abundant paralog among the anoctamin family members and is involved in modulating the scramblase activity in platelets in disease such as Scott syndrome as described above. Ano9 may be unique because Ano1 conductance has been reported to be largely inhibited by coexpression of Ano9 [17], suggesting that it has a regulatory role in CaCC conductance natively in cells that it is expressed.

As a first step toward detailed studies of anoctamin structure and function, mAno9 and hAno6 gene were cloned, epitoped tagged at their C-terminus with green fluorescent protein (GFP) or hemagglutinin (HA), and heterologous

expression of anoctamin was analyzed in Human Embryonic Kidney (HEK) 293 cells by fluorescence microscopy and by western blotting.

Materials and Methods

Reverse Transcription-PCR

Submandibular gland tissue was collected from female B6D2F1 mouse and total RNA was extracted by TRIzol® reagent (Invitrogen, Carlsland, CA, USA). Five micrograms of total RNA were combined with oligo (dT) primers and Moloney Murine Leukemia Virus (M-MLV) reverse transcriptase (Promega, Madison, WI, USA) at 42℃ for one hour to synthesize cDNA.

cDNA template was then combined with Phusion® High-Fidelity DNA polymerase, 10mM dNTPs, 5X Phusion® HF Buffer (Finnzymes, Keilaranta, Finland), and distilled water for PCR and reaction condition was designed according to the touchdown PCR technique [29]. The reaction was initially denatured at 94℃ for 5 minutes, and subsequently put through amplification cycle consisting of denaturing for 30 seconds at 94℃, annealing for 30 seconds at annealing temperature that began at 72℃ and then decreased by 0.5℃ with each cycle, and elongation for 3 minutes at 72℃; the amplification cycle was repeated for 35 times. Primer sequences are listed in Table 2.

Table 2 Oligonucleotides used as PCR primers. Notation of 1 and 2 refers to Figure 9.

Target	Number	Direction	Oligonucleotide sequence (5'→3')
mAno9	ON-113	Forward	AAAGCGGCCGCACCATGCAGGATGATGAGAGTT
	ON-114	Reverse	AAATCTAGACTATACATCCGTGCTCCTGGAACT
hAno6	ON-151	Forward	AAACTCGAGACCATGAAAAAGATGAGCAGGAA
	ON-152	Reverse	AAATCTAGATTATTCTGATTTTGGCCGTAAATTG
mAno9-EGFP	ON-113	Forward 1	AAAGCGGCCGCACCATGCAGGATGATGAGAGTT
	ON-193	Reverse 1	TCGCCCTTGCTCACCATTACATCCGTGCTCCT
	ON-194	Forward 2	TTCCAGGAGCACGGATGTAATGGTGAGCAAGGGC
	ON-117	Reverse 2	AAAGGGCCCTTACTTGTACAGCTCGTCCATGC
hAno6-EGFP	ON-151	Forward 1	AAACTCGAGACCATGAAAAAGATGAGCAGGAA
	ON-191	Reverse 1	TCGCCCTTGCTCACCATTTCTGATTTTGGCCG
	ON-192	Forward 2	TACGGCCAAAATCAGAAATGGTGAGCAAGGGC
	ON-117	Reverse 2	AAAGGGCCCTTACTTGTACAGCTCGTCCATGC
hAno6-HA	ON-151	Forward	AAACTCGAGACCATGAAAAAGATGAGCAGGAA
	ON-179	Reverse	AAATCTAGACTATGCATAGTCCGGGACGTCAT-AGGGATATGCTTCTGATTTTGGCCGTAAATTG

Ligation and subcloning into mammalian expression plasmids

The PCR product was electrophoretically seperated on 0.8% agarose gel. The band of anticipated size was cut and eluted by Dual PCR purification kit (Bionics, Seoul, Korea).

The target gene was inserted into expression vector, pcDNA3.1(+), following digest with restriction enzymes (ELPIS-Biotech, Daejeon, Korea), and ligated by T4 DNA Ligase (ELPIS-Biotech, Daejeon, Korea). Then the plasmid was transformed into CCC(Competent Cells for cloning) – TOP10 (iNtRON Biotechnology, Gyeonggi-do, Korea) by heat shock at 42℃ for 50 seconds. From the transformed bacteria that colonized on the ampicillin-added LB plate, plasmid DNA was extracted with Dokdo-Prep™ Plasmid DNA Mini-prep kit (Elpis Biotech, Seoul, Korea) and concentration of the prepared plasmid DNA was quantified by

Nanodrop® (ND-1000 Spectrophotometer). Confirmation of cloning was done by diagnostic restriction digest analysis. Finally, DNA sequencing was performed through commercial DNA sequencing services (Macrogen, Seoul, Korea).

HEK Transfection

HEK293 cell was incubated in Dulbecco's modified Eagle's medium (DMEM) (Welgene, Daegu, Korea) with 10% fetal bovine serum (FBS) (PAA, Linz, Austria) and 1X penicillin/streptomycin (Gibco, Rockville, MD, USA) at 37℃ and 5% CO_2 condition. Cell was transfected by calcium-phosphate method. Calcium-DNA solution was prepared with 125mM $CaCl_2$, 2X BES (*N*,*N*-bis[2-hydroxyethyl]-2-aminoethanesulfonic acid)-buffered saline (BBS) (280mM NaCl, 1.5mM Na_2HPO_4, 50mM BES, pH 6.96), and 5μg of DNA. The solution was incubated at room temperature for 15 minutes. Two hundred micro liter of the solution was mixed with 7.5 X 10^5 cells, and added dropwise on plate containing fresh media. After 18 hours of incubation at 35℃ and 3% CO_2 condition, media was changed to DMEM and incubated at 37℃, 5% CO_2 condition for 48 hours.

Fluorescence Microscopy

Transfected HEK293 cell was detached by trypsin-ethylenediaminetetraacetic acid (EDTA) (Gibco) after 48 hours and transferred to a cover glass coated with poly-D-lysine (Trevigen, Gaithersburg, MD, USA). It was fixed with 4% (w/v) paraformaldehyde at 4℃ for 20 minutes, washed with 1X phosphate buffered saline (PBS) for three times, and mounted on slide glass by Mounting Media (Biomeda, Foster City, CA, USA). Fluorescence was detected by confocal laser scanning microscope, Olympus-FV300 (Olympus, Tokyo, Japan).

Western blotting

The transfected HEK293 cell was lysed by 25mM trisaminomethane (Tris)-HCl (pH 7.4), 1mM ethyleneglycol tetraacetic acid (EGTA), and 1X protease inhibitor cocktail (Bionics). It was centrifuged at 1,000g for 5 minutes for nucleus to be pellet. The supernatant was centrifuged at 23,000g for 15 minutes which led cell membrane part to be pellet and cytosolic protein to remain in the supernatant, which was stored. Membrane part was resuspended in 25mM Tris-HCl (pH 7.4), 150mM NaCl, 5mM EDTA (pH 8.0), 0.05% NaAzide, 1% Triton X-100, 1mM EGTA and 1X protease inhibitor cocktail solution and rotated to mix at 4℃. After 18 hours, it was centrifuged at 23,000g for 5min to collect membrane protein in supernatant and to remove insoluble debris.

Cytosolic protein and membrane protein were separately run on 10% sodium dodecyl sulfate polyacrylamide gel electrophoresis (SDS-PAGE) and transferred to polyvinylidene fluoride (PVDF) membrane (Dogen, Seoul, Korea). The membrane was blocked by 5% skim milk for one hour to inhibit nonspecific binding, and then washed with PBS-T (PBS + 0.1% Tween-20) 3 times. Then it was treated with rabbit anti-GFP antibody (AbFrontier, Seoul, Korea) for one hour and anti-rabbit antibody (Invitrogen) for an hour in order. Horseradish peroxidase (HRP) conjugated to the secondary antibody was activated by enhanced chemiluminescence (ECL) detection kit (Intron) and it was detected by Fuji Fujifilm Las-1000 Luminescent Image Analyzer.

Results

mAno9 Gene Cloning

From mouse submandibular gland cDNA, mAno9 gene was amplified by PCR. The band of 2.2 kilobase (kb) that corresponded to the predicted size of mAno9 (2244bp) was isolated and purified (Figure 6a). To subclone, mAno9 DNA and vector, pcDNA3.1 (+), were digested with NotI and XbaI and purified (Figure 6b). Enzymatic restriction site of pcDNA3.1 (+) vector and inserted genes are shown in Figure 7a.

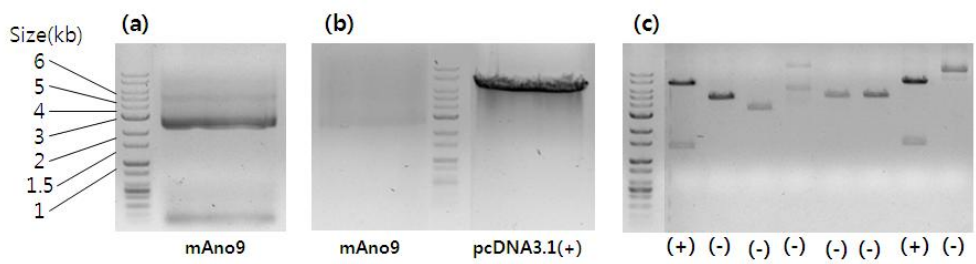

Figure 6 mAno9 cloning (a) PCR product that shows the expected band at 2.2kb. (b) Purification of digested insert and vector for ligation. (c) Diagnostic analysis to assess cloning. (+) indicates success while (-) means unsuccess with respect to the restriction digest analysis (Figure 7b).

Among tens of bacterial colonies on ampicillin-added LB plate, 32 of them were randomly chosen and plasmid DNAs were minipreped to determine positive transformants by restriction digest analysis. As shown in Figure 6c, the 1st and the 7th colonies were the positive that showed the two expected bands of 6.4kb and 1.3kb sizes. Overall, there were 5 out of 32 bacterial colonies that had been positively transformed by mAno9-inserted vector. Finally, DNA sequencing was performed for one of the five samples.

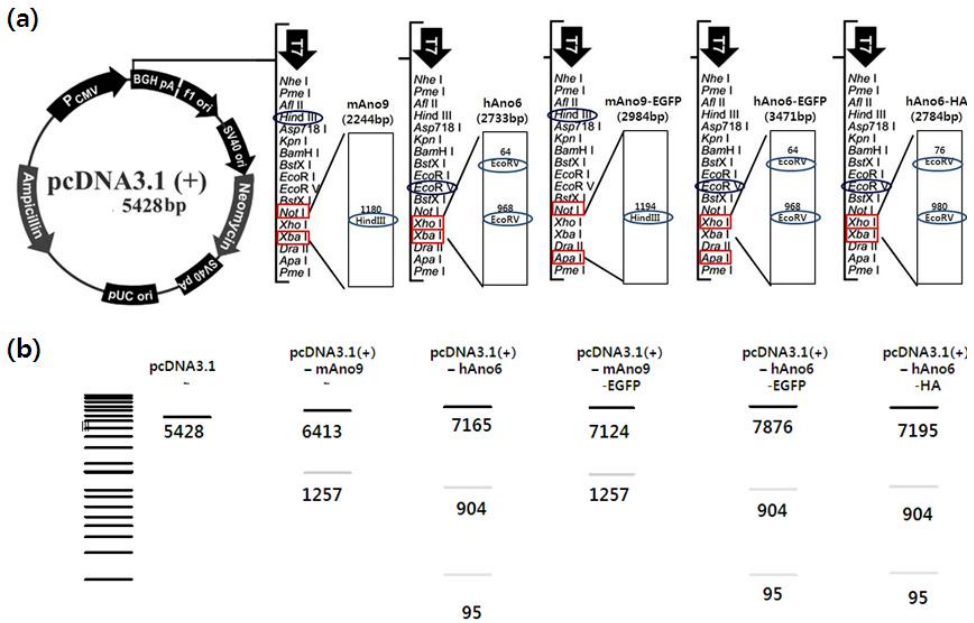

Figure 7 Scheme for subcloning (a) Map of pcDNA3.1(+) is shown and enzymatic sites are enlarged. Red rectangles indicate restriction sites of the vector where to be ligated with insert. Blue ovals note restriction sites used for restriction digest analysis. The numbers above blue ovals on the Ano show the location of digestion sites. (b) Scheme of restriction digest analysis to diagnose each plasmid whether each is inserted with target gene. Empty pcDNA3.1(+) shows one band whereas the inserted ones show two or three bands.

hAno6 Gene Cloning

Gel electrophoresis data are shown orderly in Figure 8. From the PCR product, size of 2.7kb band that corresponded to the expected size of hAno6 (2733bp) was isolated and purified (Figure 8a). To subclone, pcDNA3.1(+) and hAno6 DNA were digested with XbaI and XhoI (according to Figure 6a) and purified (Figure 8b).

Among tens of bacterial colonies on ampicillin-added LB plate, 32 of them were randomly chosen and plasmid DNAs of them were minipreped. In the

restriction digest analysis with EcoRV, empty vector was expected to turn up to one band at 5428bp, whereas the inserted vector would show three bands at 7165, 904, and 95bp (Figure 7b). Figure 8c presents a quarter of the result of restriction digest analysis. Three out of 32 samples came out as two bands at 7.2kb and 0.9kb size, which meant the bacteria had been transformed by hAno6-inserted vector. Expected band at 95bp was too small in size to be detected. Finally, DNA sequencing was performed for one of the three samples.

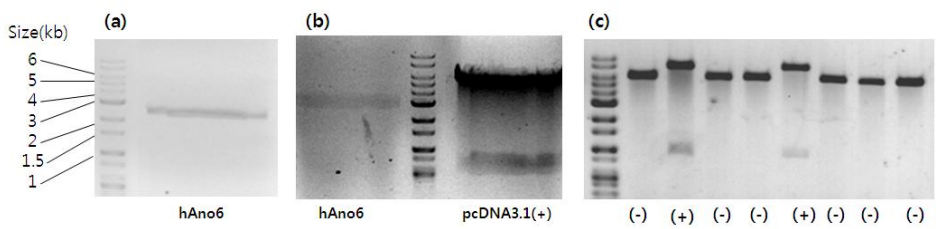

Figure 8 hAno6 cloning (a) PCR product that shows the expected band at 2.7kb. (b) Purification of digested insert and vector for ligation. (c) Diagnostic analysis to assess cloning. (+) indicates success while (-) means unsuccess with respect to the restriction digest analysis.

GFP Tagging

mAno9-EGFP

GFP was appended to the C-terminus of mAno9 and hAno6 gene. As GFP can be visualized under the fluorescence microscope, the expression of target gene can be assessed by this method.

mAno9 inserted vector (pcDNA3.1(+)-mAno9) prepared from above was linearized with restriction enzyme, NdeI, and used as a template to append EGFP tag to mAno9. pEGFP-N2 vector served as a source for Enhanced GFP (EGFP) gene and overlap PCR method was used to link EGFP to C-terminus of mAno9.

Primers were designed with respect to the scheme of overlap PCR shown in Figure 9. In case of reverse primer 1, it was designed to have annealing site for Ano at its 5' end and dangling 3' sequence which would connect fragment of EGFP to Ano at the first round of overlap PCR. Similarly, forward primer 2 had annealing site for EGFP at its 3' end and dangling 5' sequence that would conncect fragment of Ano to EGFP. PCR products of EGFP fragment-appended mAno9 ('Ano / EGFP-fragment' in Figure 9a) and mAno9 fragment-appended EGFP ('EGFP / Ano-fragment' in Figure 9a) are shown in Figure 10a.

At the second round of overlap PCR, the two PCR products that have appended sites from the first round were gel-purified and used as template. Annealing of complementary sequences engineered into respected PCR primers that amplified the first round PCR products and using outside primers to amplify the complete second round of overlap PCR of the mAno9 fragment with appended EGFP at C-terminus (mAno9-EGFP) is shown in Figure 10b.

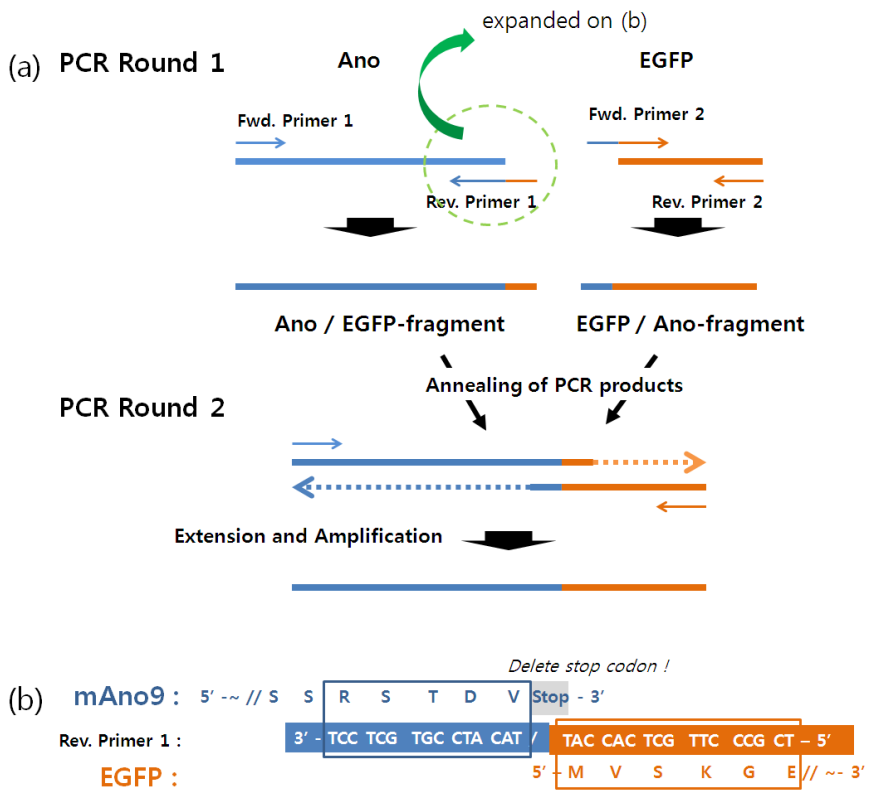

Figure 9 Scheme for overlap PCR (a) At the first round, dangling primers anneal to the DNA, which will result in elongated Ano with EGFP-fragment and EGFP with Ano-fragment. They anneal each other at the second round and EGFP linked Ano is acquired after overlap PCR. (b) Example of primer designing. The encircled area in (a) is expanded in case of mAno9. The primer has annealing site for mAno9 and dangling sequence, which would connect fragment of EGFP to mAno9.

To subclone, mAno9-EGFP and pcDNA3.1 (+) were restricted with NotI and ApaI (according to Figure 7b), and purified on agarose gel (Figure 10c).

Among tens of colonies of bacteria on ampicillin-added LB plate, 16 of them were randomly chosen and plasmid DNAs of them were minipreped. One out of 16 samples came out as two bands at 7.1kb and 1.3kb size, which meant the bacteria had been successfully transformed. Figure 10d presents representatives of

successful and unsuccessful transformation with respect to the restriction digest analysis by HindIII (Figure 7b). Finally, DNA sequencing was performed.

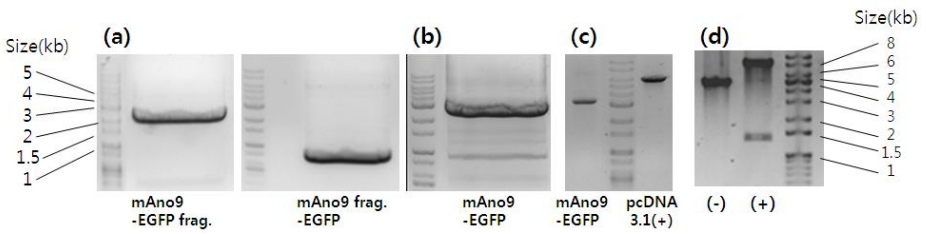

Figure 10 mAno9-EGFP subcloning (a) PCR products from the first round PCR. (b) PCR product from the second round PCR. (c) Purification of digested insert and vector for ligation. (d) Diagnostic analysis of restriction with HindIII. (+) indicates success while (-) means unsuccess with respect to the restriction digest analysis (Figure 7b).

hAno6-EGFP

hAno6 inserted vector (pcDNA3.1(+)-hAno6) prepared from previous step was linearized with restriction enzyme, BglIII, and used as a template for hAno6. pEGFP-N2 vector served as a source for Enhanced GFP (EGFP) gene.

PCR products from first round (hAno6 – EGFP fragment and hAno6 fragment -EGFP) are shown in Figure 11a and final product of overlap PCR is shown in Figure 11b. To subclone, hAno6-EGFP and pcDNA3.1(+) were restricted with XhoI and ApaI (Figure 7b) and purified on agarose gel (Figure 11c).

Among tens of colonies of bacteria on ampicillin-added LB plate, 16 of them were randomly chosen and plasmid DNAs of them were minipreped. Three out of 16 samples came out to have been successfully transformed. Figure 11d presents representatives of successful and unsuccessful transformation with respect to the restriction digest analysis by EcoRV (Figure 7b). Finally, DNA sequencing was performed.

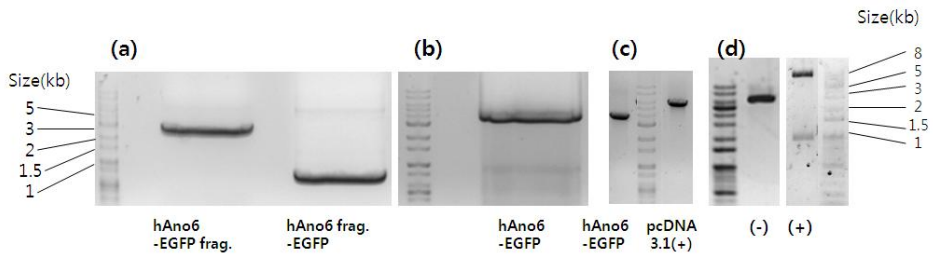

Figure 11 hAno6-EGFP subcloning (a) PCR products from the first round PCR. (b) PCR product from the second round PCR. (c) Purification of digested insert and vector for ligation. (d) Diagnostic analysis of restriction with EcoRV. (+) indicates success while (-) means unsuccess with respect to the restriction digest analysis (Figure 7b).

Hemagglutinin (HA) tagging

HA-tag that codes for amino acid sequence of YPYDVPDYA (single letter codes for amino acid residues) was linked to 3'-terminus of hAno6 gene. HA-tag is used usually to facilitate the detection, isolation, purification of the proteins, and identification of interactions between proteins by allowing antibody for HA can specifically bind to hAno6-HA.

As HA tag has size of 27bp, the appending was conducted by designing reverse primer to have HA-tag gene region at the 5'-terminus of itself (Figure 12).

Figure 12 Scheme for HA tagging. Reverse primer has a dangling sequence to be a HA tag.

HA-tagged hAno6 gene was prepared from PCR (Figure 13a). To subclone, hAno6-HA and pcDNA3.1(+) were restricted with XhoI and XbaI (according to Figure 7b) and purified on agarose gel (Figure 13b).

Among tens of bacterial colonies on ampicillin-added LB plate, 16 of them were randomly chosen and plasmid DNAs of them were minipreped to find out transformed one. Fourteen out of 16 samples came out to have been successfully transformed. Figure 13c presents representatives of successful and unsuccessful transformation with respect to the restriction digest analysis by EcoRV (according to Figure 7b). Finally, DNA sequencing was performed.

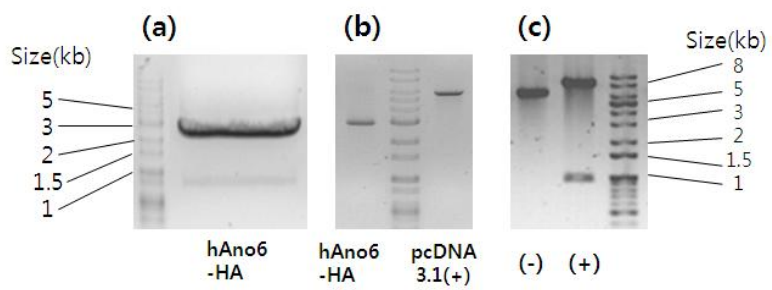

Figure 13 hAno6-HA subcloning(a) PCR products purification. (b) Digested insert and vector purification for ligation. (c) Diagnostic analysis to assess cloning. (+) indicates success while (-) means unsuccess with respect to the restriction digest analysis (Figure 7b).

Consequently, mAno9 and hAno6 gene were cloned, and epitope tagged with EGFP or HA-tag, and subcloned into mammalian expression vector, pcDNA3.1 (+).

Transfection and protein expression

Ano-EGFP plasmids were transfected into HEK293 cell in order to verify whether they are heterologously expressed in mammalian cell. The subcellular localization was also determined because the isoform-specific location in cells may serve as a clue about the function of mAno9 and hAno6 isoforms.

After incubation of transfected HEK293 cell for 48 hours, sufficient fluorescence from expressed EGFP was detected (Figure 14). Images from confocal laser scanning microscopy showed that mAno9 was localized intracellularly, whereas hAno6 was expressed in both membrane and intracellular part (Figure 15).

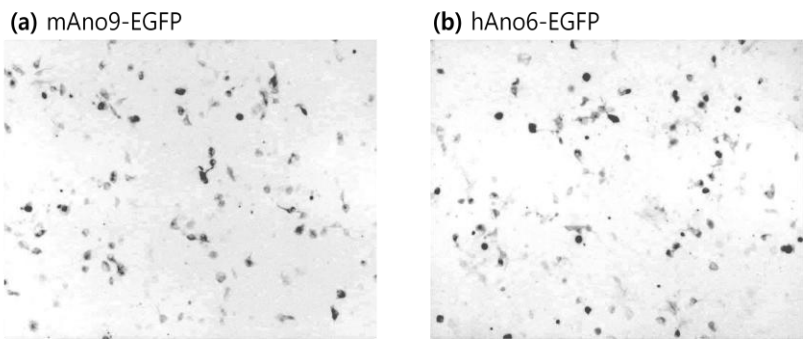

Figure 14 Fluorescence from EGFP after 48 hours of incubation.

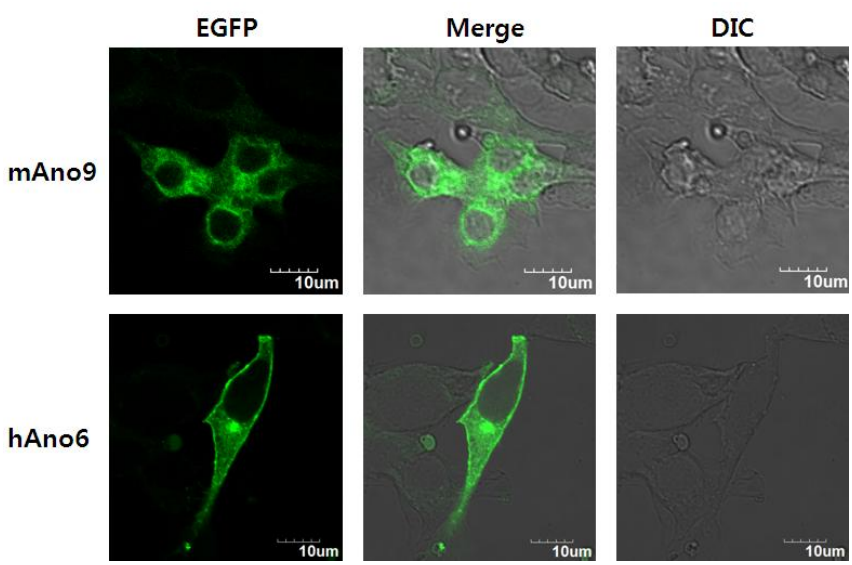

Figure 15 Confocal image**.** Leftmost column shows detected EGFP and rightmost column exhibits image of differential interference contrast (DIC). They are merged in middle column to indicate the location of EGFP in single cell.

Western blotting

Through western blotting, EGPF can be specifically detected and it helps clarify whether expressed EGFP is translated into full-length Ano-EGFP proteins. Cellular proteins were separately prepared into membrane protein fraction and cytosolic fraction to confirm the distribution of Ano-EGFP protein.

Calculated from mRNA sequences of open reading frame, expected protein sizes of mAno9-EGFP and hAno6-EGFP were 114kDa and 130kDa, respectively. From western blotting data, specific signal was detected from only membrane part of mAno9-transfected HEK293 cell at 180kDa which was bigger than the anticipated one (Figure 16). There was no specific signal of hAno6 from neither membrane nor cytosolic fraction.

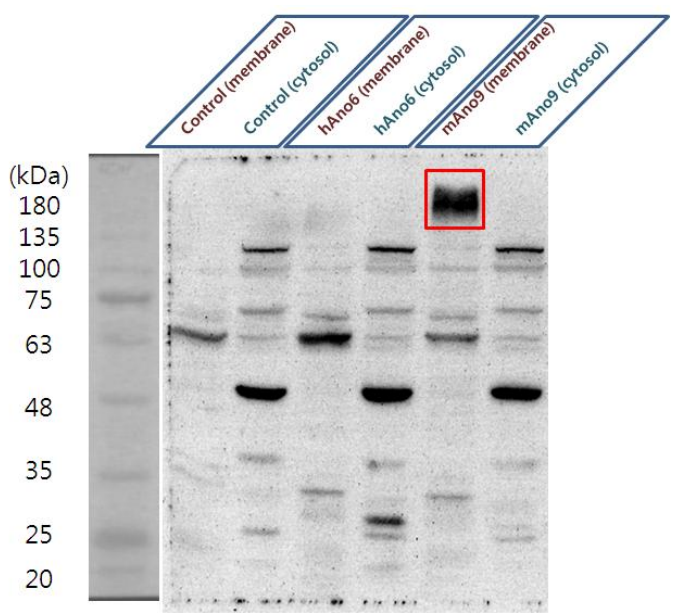

Figure 16 Western blotting data shows specific signal only at membrane protein part of mAno9 transfected HEK293 cell.

Discussion

As a part of investigation of role and function of anoctamin family, mAno9 and hAno6 gene were cloned and EGFP or HA-tag was linked to them. mAno9-EGFP and hAno6-EGFP were heterologously expressed in HEK293 cell and fluorescence was observed. Additionally, HA-tag was linked to hAno6 so as to the antibody for HA could specifically bind to hAno6-HA.

To summarize the main finding of this thesis, mAno9 and hAno6 were successfully cloned from cDNA of mouse submandibular gland and HEK293 cell line, respectively. Cloned mAno9 had size of 2244 bp and hAno6 had size of 2733 bp and they corresponded to open reading frame of mRNA sequence of Mus musculus anoctamin 9 (NCBI Reference Sequence: NM_178381.3) and Homo sapiens anoctamin 6, transcript variant 1 (NCBI Reference Sequence: NM_001025356.2).

Heterologous expressions of mAno9-EGFP and hAno6-EGFP in HEK393 showed measurable fluorescence after 24 hours of incubation and the intensity increased gradually until approximately 20% of transfectants showed fluorescence after 48 hours.

mAno9-EGFP was localized intracellularly in confocal microscope image as fluorescent diffusely dispersed inside cell and did not show any clear lining. Considering the fact that Ano9 has been reported to inhibit conductance of Ano1 which function at the plasma membrane, Ano9 might interact with intracellular part of Ano1 during protein folding and/or maturation steps in the endoplasmic reticulum or the Golgi either directly or through additional intermediary proteins. Additional protein-protein interaction studies are needed to clarify this issue.

Western blotting image showed a distinctive band at 180kDa from the membrane fraction of mAno9 proteins. Calculated protein size from open reading

frame of mAno9-EGFP is 114kDa and there was size discrepancy of 66kDa. The discrepancy might have happened due to post-translational modification involving addition of functional groups such as glycosylation, or ubiquitination.

The facts that fluorescence was detected intracellularly and western blotting signal was found in membrane fraction suggest that mAno9 is localized at not plasma membrane but intracellular organellar membrane. Membrane proteins are usually involved in structure, adhesion, receptor, and transport. As there are many enclosed organelles, more specific localization is needed to figure out what kind of roles Ano9 does.

hAno6-EGFP was detected in both membrane and cytoplasm in the confocal image. Considering the fact that Ano6 is the most abundant Ano paralog [17], this result implies diverse function of Ano6 in various tissues. Calculated protein size from open reading frame was 130kDa. However, western blotting result did not show any specific band. Because fluorescence was certainly appeared and the intensity was similar to that of mAno9-EGFP, specific band was anticipated to be found. Possible errors may come from protein preparation step that could have lost hAno6-EGFP during procedure. To exclude experimental error during western blotting, it should be carefully repeated with adjustment of protein preparation steps especially centrifugal conditions.

As Ano9 and Ano6 were found to be expressed in mouse salivary gland [17], they may perform certain roles in the tissue. The roles need to be clarified by further study such as finding existence of interacting proteins, measuring electrophysiologic nature, identifying different phenotype under upregulation or downregulation. After their role and functional mechanism are cleared, they might be used as therapeutic targets for saliva-related diseases.

Conclusion

mAno9 and hAno6 were cloned from cDNA of mouse submandibular gland tissue and HEK293 cell line. They were inserted into mammalian expression vector and heterologously expressed in HEK293 cell. With aid of EGFP linked to N-terminus of each anoctamin protein, their expression was assessed with fluorescence microscope. Confocal laser scanning image showed that mAno9 was localized intracellularly, whereas hAno6 was expressed in both cytoplasm and plasma membrane. Western blotting data showed distinctive signal for mAno9 at only membrane protein fraction, but no specific signal for hAno6 from neither membrane nor cytosolic fraction and the result needs to be verified with additional experiments.

References

1. Lee, G., Y. Yu, and H. Lee, *Saliva*, in *Oral Biochemistry*, B.-M. Min, Editor. 2007, DaehanNarae Publishing: Seoul.
2. Darvell, B.W. and R.K. Clark, *The physical mechanisms of complete denture retention.* Br Dent J, 2000. **189**(5): p. 248-52.
3. Guggenheimer, J. and P.A. Moore, *Xerostomia: etiology, recognition and treatment.* J Am Dent Assoc, 2003. **134**(1): p. 61-9; quiz 118-9.
4. Lee, M.G., et al., *Molecular mechanism of pancreatic and salivary gland fluid and HCO3 secretion.* Physiol Rev, 2012. **92**(1): p. 39-74.
5. Arreola, J., J.E. Melvin, and T. Begenisich, *Activation of calcium-dependent chloride channels in rat parotid acinar cells.* J Gen Physiol, 1996. **108**(1): p. 35-47.
6. Flores, C.A., et al., *TMEM16 proteins: the long awaited calcium-activated chloride channels?* Braz J Med Biol Res, 2009. **42**(11): p. 993-1001.
7. Marty, A., Y.P. Tan, and A. Trautmann, *Three types of calcium-dependent channel in rat lacrimal glands.* J Physiol, 1984. **357**: p. 293-325.
8. Caputo, A., et al., *TMEM16A, a membrane protein associated with calcium-dependent chloride channel activity.* Science, 2008. **322**(5901): p. 590-4.
9. Schroeder, B.C., et al., *Expression cloning of TMEM16A as a calcium-activated chloride channel subunit.* Cell, 2008. **134**(6): p. 1019-29.
10. Yang, Y.D., et al., *TMEM16A confers receptor-activated calcium-dependent chloride conductance.* Nature, 2008. **455**(7217): p. 1210-5.
11. Romanenko, V.G., et al., *Tmem16A encodes the Ca2+-activated Cl- channel in mouse submandibular salivary gland acinar cells.* J Biol Chem, 2010. **285**(17): p. 12990-3001.
12. Hartzell, H.C., et al., *Anoctamin/TMEM16 family members are Ca2+-activated Cl- channels.* J Physiol, 2009. **587**(Pt 10): p. 2127-39.
13. Kunzelmann, K., et al., *Anoctamins.* Pflugers Arch, 2011. **462**(2): p. 195-

208.

14. Duran, C., et al., *Chloride channels: often enigmatic, rarely predictable.* Annu Rev Physiol, 2010. **72**: p. 95-121.
15. Kunzelmann, K., et al., *Bestrophin and TMEM16-Ca(2+) activated Cl(-) channels with different functions.* Cell Calcium, 2009. **46**(4): p. 233-41.
16. Desper, R. and O. Gascuel, *Theoretical foundation of the balanced minimum evolution method of phylogenetic inference and its relationship to weighted least-squares tree fitting.* Mol Biol Evol, 2004. **21**(3): p. 587-98.
17. Schreiber, R., et al., *Expression and function of epithelial anoctamins.* J Biol Chem, 2010. **285**(10): p. 7838-45.
18. Pifferi, S., M. Dibattista, and A. Menini, *TMEM16B induces chloride currents activated by calcium in mammalian cells.* Pflugers Arch, 2009. **458**(6): p. 1023-38.
19. Suzuki, J., et al., *Calcium-dependent phospholipid scrambling by TMEM16F.* Nature, 2010. **468**(7325): p. 834-8.
20. Leventis, P.A. and S. Grinstein, *The distribution and function of phosphatidylserine in cellular membranes.* Annu Rev Biophys, 2010. **39**: p. 407-27.
21. Wielders, S.J., et al., *Absence of platelet-dependent fibrin formation in a patient with Scott syndrome.* Thromb Haemost, 2009. **102**(1): p. 76-82.
22. Zwaal, R.F., P. Comfurius, and E.M. Bevers, *Scott syndrome, a bleeding disorder caused by defective scrambling of membrane phospholipids.* Biochim Biophys Acta, 2004. **1636**(2-3): p. 119-28.
23. Carles, A., et al., *Head and neck squamous cell carcinoma transcriptome analysis by comprehensive validated differential display.* Oncogene, 2006. **25**(12): p. 1821-31.
24. West, R.B., et al., *The novel marker, DOG1, is expressed ubiquitously in gastrointestinal stromal tumors irrespective of KIT or PDGFRA mutation status.* Am J Pathol, 2004. **165**(1): p. 107-13.
25. Carneiro, A., et al., *Prognostic impact of array-based genomic profiles in esophageal squamous cell cancer.* BMC Cancer, 2008. **8**: p. 98.

26. Huang, X., et al., *Comprehensive genome and transcriptome analysis of the 11q13 amplicon in human oral cancer and synteny to the 7F5 amplicon in murine oral carcinoma.* Genes Chromosomes Cancer, 2006. **45**(11): p. 1058-69.
27. Das, S., et al., *NGEP, a prostate-specific plasma membrane protein that promotes the association of LNCaP cells.* Cancer Res, 2007. **67**(4): p. 1594-601.
28. Dutertre, M., et al., *Exon-based clustering of murine breast tumor transcriptomes reveals alternative exons whose expression is associated with metastasis.* Cancer Res, 2010. **70**(3): p. 896-905.
29. Korbie, D.J. and J.S. Mattick, *Touchdown PCR for increased specificity and sensitivity in PCR amplification.* Nat Protoc, 2008. **3**(9): p. 1452-6.

국문초록

아녹타민 아형의 클로닝과 이종발현 연구

아녹타민 1 은 타액 분비에 중요한 역할을 하는 칼슘-활성화 염소 이온 채널의 성질을 가지고 있음이 최근에 알려지면서 주목을 받게 되었다. 아녹타민 군에는 9 가지의 다른 아형들이 존재하나 이들에 성질에 대해서는 아직 많이 알려진 바가 없다. 이 연구에서는 생쥐 아녹타민 9 와 인간 아녹타민 6 에 대해 알아보기 위해 이 유전자들을 클로닝하고, C-말단에 EGFP (enhanced green fluorescent protein) 혹은 HA (hemagglutinin) 에피토프를 연결한 후, HEK293 세포에 이종발현을 시켰다. EGFP 가 연결된 아녹타민의 형광을 관찰해 발현 위치를 확인하고, 세포로부터 단백질을 추출해서 EGFP 특이적 항원으로 아녹타민을 검출하였다. 그 결과, 쥐 아녹타민 9 과 인간 아녹타민 6 발현 플라스미드는 모두 HEK293 세포에서 이종발현 되었고, 쥐 아녹타민 9 은 세포 내에 국한되었으나 인간 아녹타민 6 는 세포막과 세포 내에서 모두 발현되었다. 이 사실을 통해 아녹타민 아형들은 세포 내 특정 부위에서 고유의 역할을 할 것이라 추측되며 이를 더 자세히 알아보기 위해 추후의 많은 연구가 필요할 것이다.

주요어 : 아녹타민, 칼슘-활성화 염소 채널, 클로닝, 이종발현
학번 : 2009-22686